Journal of Solid State Chemistry 184 (2011) 2713–2718

Contents lists available at ScienceDirect

Journal of Solid State Chemistry

journal homepage: www.elsevier.com/locate/jssc

Spectroscopic properties of Nd^{3+} ions in nano-perovskite $CaTiO_3$

K. Lemański, A. Gągor, M. Kurnatowska, R. Pązik, P.J. Dereń *

Institute of Low Temperature and Structure Research, Polish Academy of Sciences, Okólna 2 street, P.O. Box 1410, 50-950 Wrocław, Poland

ARTICLE INFO

Article history:
Received 17 February 2011
Received in revised form
3 August 2011
Accepted 7 August 2011
Available online 11 August 2011

Keywords:
Nanocrystals
$CaTiO_3$
Neodymium
Luminescence

ABSTRACT

In this work, we present for the first time the spectroscopic properties of perovskite nanocrystals $CaTiO_3$: Nd^{3+}, measured at room and liquid nitrogen temperature. Samples were prepared by the sol–gel method and annealed at 700 and 1000 °C. The concentration of Nd^{3+} ranged from 0.5% to 5%. Average nanocrystallite size primarily depends on the annealed temperature and is about 25 and 50 nm for 700 and 1000 °C, respectively. The absorption, emission and excitation spectra (monitored at 1078 nm) as well as the decay time profile of the emission from the $^4F_{3/2}$ energy level of Nd^{3+} are obtained. The increasing amount of Nd^{3+} ions decreases the lifetime of the $^4F_{3/2}$ level and that changes from 146 μs for 0.5% to 50 μs for 5% of Nd^{3+} concentration. The strongest emission was observed at two regions: 1050–1120 nm and 865–930 nm and was assigned to the $^4F_{3/2}\rightarrow{}^4I_{11/2}$ and $^4F_{3/2}\rightarrow{}^4I_{9/2}$ transitions, respectively. The spectroscopic quality parameter of neodymium in the $CaTiO_3$ lattice has been calculated from the emission spectra. The influence of luminescent properties depending on the annealing temperature and concentration of neodymium ions is discussed.

1. Introduction

Study of nano-sized materials has become very important recently. New developments in electronics, optics or biology imply the evolution of new phosphors whose properties can be optimized by reaching the nanometric scale.

Nanocrystallites possess unique properties, which are not observed for corresponding bulk samples. Their size, shape and big surface to volume ratio influence material properties, such as for example electronic energy levels, conductivity and phase transition temperatures [1].

$CaTiO_3$ is a well known perovskite used for different applications. This titanate is a chemically and thermally stable and possesses a good mechanical resistance and stability [2]. Some valuable features make this perovskite a candidate for a new phosphor or even a new host for powder lasers. The refractive index of $CaTiO_3$ is high—2.4 (for 632 nm) [3], and it has a melting point of 2220 K [4]. High permittivity and low dielectric losses make this crystal a suitable candidate for microwave applications [5]. $CaTiO_3$ is already used in electronic ceramic materials [6] and as thin films for electroluminescent devices, amongst others because of its low charge density. This perovskite can be also used as a component of sensors [7] or as a material for biomedical applications [8].

$CaTiO_3$ has also been used as a host for efficient luminescence of rare earth ions. Doped with praseodymium ions it exhibits strong red luminescence under UV excitation [9]. The structure of "ideal" perovskite is cubic with the space group *Pm*3*m*. At room temperature $CaTiO_3$ possesses lower orthorhombic symmetry with a quadrupled unit cell and *Pbnm* space group [10]. Neodymium ions which are doped into $CaTiO_3$ replace Ca^{2+} ions in the C_s symmetry sites, because of similar ionic radius (0.148 and 0.141 nm for Ca^{2+} and Nd^{3+} ions, respectively). Valence mismatch introduces distortion of the crystal structure and creates vacancies.

Crystals doped with neodymium are one of the most useful sources of infrared radiation. Practical applications of this radiation mainly occurs in the medical field, processing of materials or marking documents, also in IR cameras and remote controls. In the most cases, the strongest laser transition is from the $^4F_{3/2}$ to $^4I_{11/2}$ energy level of Nd^{3+}. Other transitions are also available for longer or shorter wavelengths. For higher concentrations of neodymium a possible luminescence quenching caused by nonradiative processes occurs. This is the reason why the commercially available laser crystals based on the radiation of neodymium, like YAG, YVO_4 and $YAlO_3$, are doped with a small amount of neodymium, usually 1%. Recently, another material appeared to be a good host for Nd^{3+} ions; namely $LaAlO_3$ perovskite [11].

Two years ago, Marquesa et al. [12] discussed optical properties of $CaTiO_3$: Nd^{3+} micropowders, but they did not report any emission spectra. Therefore we believe that in this paper we present for the first time the luminescence properties of $CaTiO_3$ nanocrystals doped with Nd^{3+} ions. The influence of luminescent properties depending on the annealing temperature and concentration of neodymium ions are discussed.

* Corresponding author.
E-mail address: P.Deren@int.pan.wroc.pl (P.J. Dereń).

0022-4596/$ - see front matter © 2011 Elsevier Inc. All rights reserved.
doi:10.1016/j.jssc.2011.08.004

2. Experimental

The samples have been prepared using the sol–gel method [13] and annealed for 8 h at 700 and 1000 °C. The concentration of Nd^{3+} ranged from 0.5% to 5%. The crystalline structure has been confirmed by X-ray diffraction (XRD) measurement. Powder diffraction data were collected on an X'Pert PRO X-ray diffraction system equipped with a PIXcel ultra-fast line detector, focusing mirror and Soller slits using Cu $K\alpha$ radiation. The diffraction patterns were collected at room temperature in reflection mode in the range of $10^\circ \le 2\theta \le 100^\circ$ using step scans of 0.026°. The crystal structures of $CaTiO_3$: 5% Nd^{3+} and $CaTiO_3$: 0.5% Nd^{3+} were refined using the Rietveld method as implemented in the Jana2000 program package [14]. The peak profiles were fitted using a pseudo-Voigt function. The model of the crystal structure was taken from [10]. The refinement was performed in the standard setting (*Pnma*) of the *Pbnm* space group. Since Nd^{3+} substitutes for Ca^{2+} the fractional coordinates for both ions were constrained to the same values (see Table 1 and Table 3 of the supplementary materials) but individual site occupation factors were determined for Nd^{3+} and Ca^{2+}. The summary site occupation factor for the Ca/Nd position was set to 1. Calculated and observed data together with a difference plot for $CaTiO_3$: 5% Nd^{3+} are presented in Fig. 1 and Table 1. Fig. 12 and Table 3 in the supplementary materials present corresponding data for $CaTiO_3$: 0.5% Nd^{3+}.

The concentration of doped Nd^{3+} ions has been confirmed by the Energy Dispersive X-ray (EDAX) analysis (see Fig. 15 of the supplementary materials).

As an excitation source we used an argon laser with the lines at 514.5 nm and for the decay time the 532 nm line from a Nd:YAG pulse laser. The emission spectra were recorded using a Jobin Yvon THR1000 monochromator with CCD camera and an InGaAs detector was used for NIR analysis. Decay profiles were obtained on a Lecroy digital oscilloscope.

Table 1
Atomic coordinates, site symmetry, site occupation factors and isotropic displacement parameters for $CaTiO_3$: 5% Nd^{3+}.

Atom	Symm.	x	y	z	s.o.f.	$U_{iso} \times 10^2$ [A^2]
Ti	C_i	0	0	0	1	0.80(4)
Ca	C_s	0.4677(2)	1/4	0.0062(5)	0.956(2)	0.87(5)
Nd	C_s	0.4677(2)	1/4	0.0062(5)	0.044(2)	0.87(5)
O1	C_s	0.5158(8)	1/4	0.5849(11)	1	0.6(2)
O2	C_1	0.2073(6)	0.0326(6)	0.2850(7)	1	0.5(2)

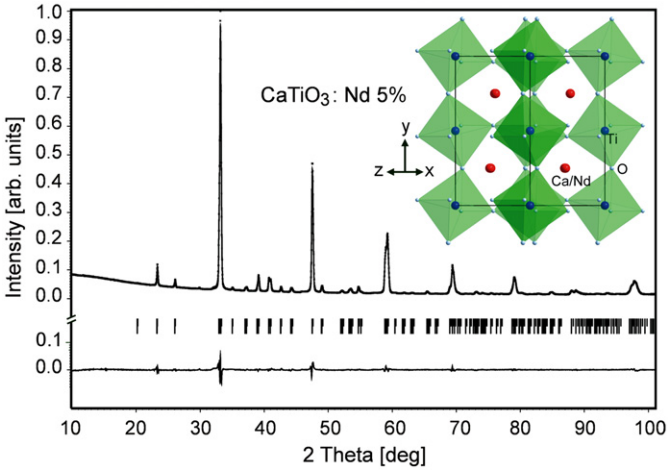

Fig. 1. Rietveld refinement results for $CaTiO_3$: 5% Nd^{3+} annealed at 1000 °C. Space group *Pnma*, $Z=4$, $a=5.446(1)$ Å, $b=7.658(1)$ Å, $c=5.396(1)$ Å. $R_p=0.029$, $R_{wp}=0.041$, $R_F=0.031$, $R_{Fw}=0.016$. The inset shows the unit cell projected in [101] direction.

3. Results and discussion

The XRD diffractograms of measured nanocrystallites, with the highest (5%) and the lowest (0.5%) amount of doped neodymium, are presented in Figs. 1 and 12, in the supplementary materials. The crystal structure of this perovskite was obtained on annealing at 700 °C .

The results of the Rietveld refinement performed for two samples annealed at 1000 °C with 0.5% and 5% concentration of Nd^{3+} show that the obtained samples are phase pure powders with a distorted perovskite structure. Despite the fact that the ionic radii of Nd^{3+} and Ca^{2+} in 12-fold coordination are comparable the lattice parameters grow with the increasing Nd^{3+} content. This is due to the valence mismatch introduced by the dopant ions, at the same time it evidences the incorporation of Nd^{3+} ions into the crystal structure. It is worth noting that refined occupancy factors for Nd^{3+} are in agreement with nominal composition. The change of lattice parameters of $CaTiO_3$: Nd^{3+} with increasing content of Nd^{3+} ions is presented in Fig. 2. Fig. 14 in the supplementary materials shows linear growth of the unit cell volume with higher concentrations of Nd^{3+}.

The results of Rietveld profile fitting are presented in Table 1 and Table 3 in the supplementary materials. The Ti–O distances are almost the same in both samples, 1.957(4) Å and 1.960(4) Å for the 0.5% and 5% samples, respectively. The mean values of the Ca/Nd–O distances are also comparable in both samples. However, there are some noticeable differences in individual Ca/Nd–O distances, (see Table 4 in the supplementary materials).

For abbreviation further in the text instead of: sample annealed at 1000 °C we will use the notation 1000 °C sample, and 700 °C sample for the sample annealed at 700 °C.

Average nanocrystallite size has been calculated using the Scherrer's [15] equation. The calculated value is around 45 nm and 30 nm for the 1000 °C and 700 °C samples, respectively (see Fig. 3). The images obtained from Transmission Electron Microscopy (TEM) and High-Resolution TEM (HRTEM) present crystallites in a nanometric scale (see Figs. 4 and 5). The images reveal the presence of small nanocrystallites of a diameter smaller than comparable to values obtained from Sherrer's formula. An amorphous phase was not visible in any samples. Selected Area

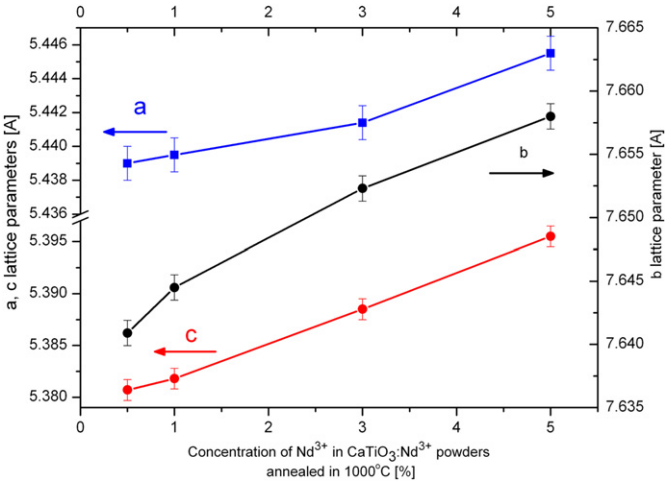

Fig. 2. The change of lattice parameters of $CaTiO_3$: Nd^{3+} with increasing content of Nd^{3+} ions.

Electron Diffraction (SAED) patterns confirm that grains are mostly mono-crystalline. Please note that term "grain" is understood to mean an agglomerate of single nanocrystals.

The 700 °C samples have similar grains for different neodymium concentrations. However, especially for the 1000 °C samples, a wide distribution of agglomerated grains occurs. Indeed, the higher temperature and thus longer time of annealing favors creating the sintered agglomerates. The surface energy of a nano-powders is high. In order to minimize their energy, crystallites form agglomerates consisting of few or more nanocrystallites. Under the influence of higher temperatures bigger agglomerated grains are formed.

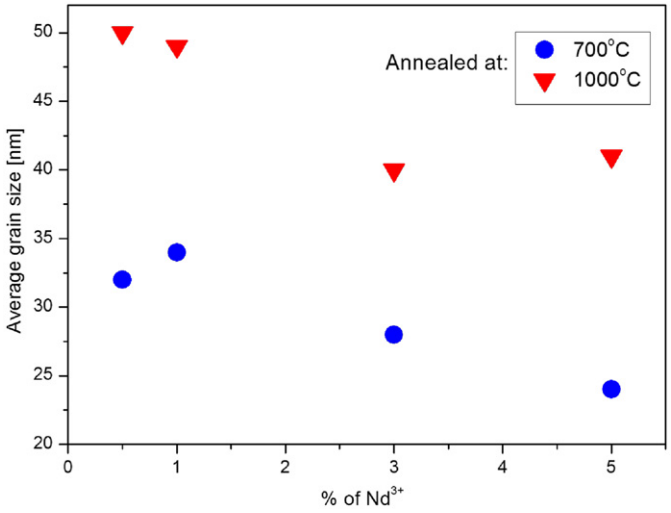

Fig. 3. Size dependence of $CaTiO_3$: Nd^{3+} nanocrystallites.

The average crystallite size was obtained from the Scherrer method, as mentioned above. From the TEM images apart from the view of the grains and the tendency of creation of agglomerates, we can also observe (especially for the 1000 °C samples), that agglomeration of nanocrystallites is lower for the samples with larger amounts of neodymium. This is due to the inhibitory influence of dopant [16] on increasing crystallite volume. Mean agglomerated grain size was calculated from the TEM images and is around 60 nm for the sample containing 0.5% of Nd^{3+} and 54 nm for the sample containing 3% of Nd^{3+}. Agglomerated grain size is in the range 100–300 nm for the $CaTiO_3$: Nd^{3+} 0.5% sample and 40–160 nm for the $CaTiO_3$: Nd^{3+} 3% sample.

The excitation spectra (see Fig. 6) have been monitored at 1078 nm, which corresponds to the $^4F_{3/2} \rightarrow {}^4I_{11/2}$ transition. Obtained peaks were assigned to the energy levels of neodymium. The laser line at 514.5 nm excites the $^4G_{7/2}$ level, which next transfers energy to the lower lying levels. However, the most intensive is the so-called hypersensitive transition $^4I_{9/2} \rightarrow {}^4G_{5/2}$, which strongly depends on the coordination of the lanthanide ion. Therefore this peak has relatively different intensities in various

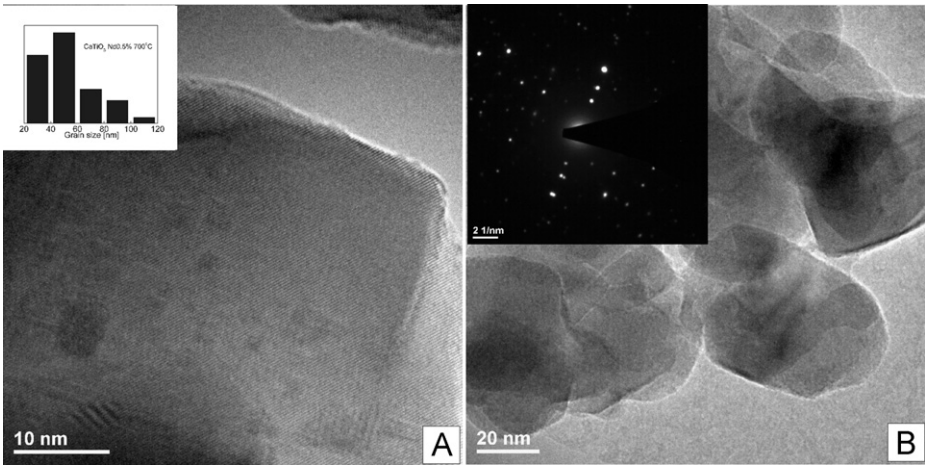

Fig. 4. (A) HRTEM image and size distribution (inset) (B) TEM image and SAED (inset) of $CaTiO_3$: 0.5% Nd^{3+} heated at 700 °C.

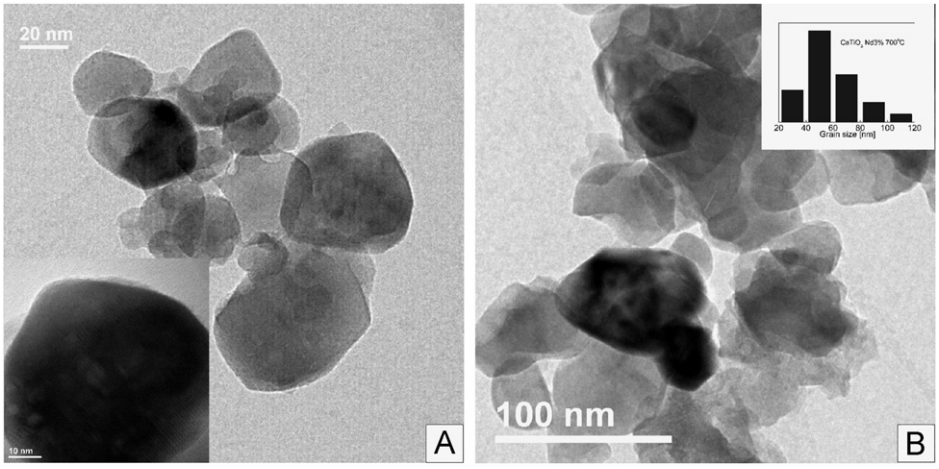

Fig. 5. (A) and (B) TEM images of sample $CaTiO_3$: Nd^{3+} heated at 700 °C. Inset (A) shows HRTEM image and inset (B) size distribution.

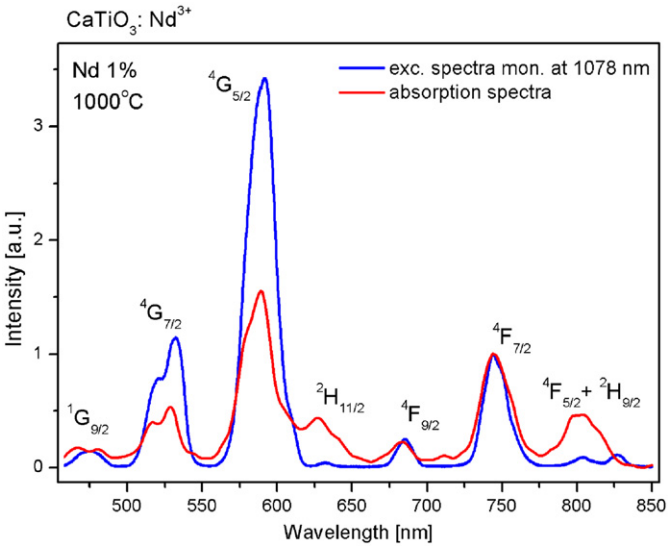

Fig. 6. The 300 K excitation and absorption spectra of $CaTiO_3$: Nd^{3+}.

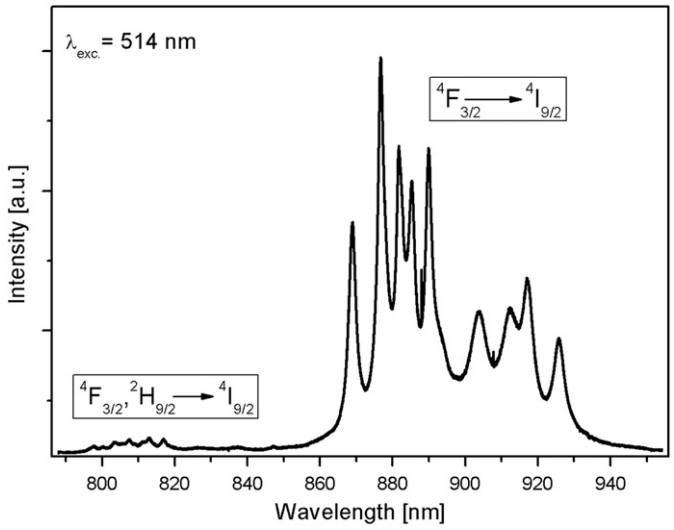

Fig. 7. The 300 K emission spectrum of sample $CaTiO_3$: 1% Nd^{3+} annealed at 700 °C.

Table 2
The energy levels of Nd^{3+} ions in $CaTiO_3$ obtained from the absorption and emission spectra.

Level of Nd^{3+}	Energies (cm^{-1})	ΔE (cm^{-1})	Number of levels	
			Theory	Exp.
$^4I_{9/2}$	0, 113, 176, 442, 606	606	5	5
$^4I_{11/2}$	1928, 2027, 2083, 2130, 2225, 2285	357	6	6
$^4I_{13/2}$	3966, 4063, 4148, 4266, 4380	414	7	5
$^4I_{15/2}$	5773, 5886, 6007, 6174, 6588, 6659, 6755	982	8	7
$^4F_{3/2}$	**11409, 11512**	103	2	2
$^4F_{5/2}+^2H_{9/2}$	12242, 12300, 12326, 12386, 12447, 12497, 12536	294	8	7
$^4F_{7/2}+^4S_{3/2}$	13337, 13442	105	6	2
$^4F_{9/2}$	14630	–	5	1
$^2H_{11/2}$	15610, 15943,	333	3	2
$^4G_{5/2}$	16976, 17270	294	3	2
$^4G_{7/2}$	18401, 18915, 19350	949	4	3
$^4K_{15/2}+^4G_{11/2}$	20800, 21415, 22463	1663	14	3
$^2P_{1/2}$	23388	–	1	1

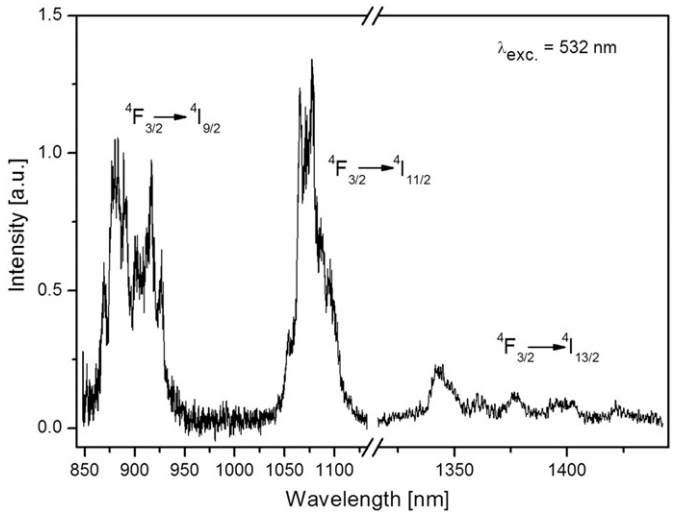

Fig. 8. The 300 K emission spectrum of $CaTiO_3$: 1% Nd^{3+} annealed at 700 °C and measured on InGaAs detector.

lattices. Energy levels obtained from the absorption and emission spectra are presented in Table 2. The transition bandwidths are much broader than in monocrystals, like for example, in $LaAlO_3$ [11]. This phenomenon could be due to the fact that active ions in polycrystalline nano-powders are placed in different environments, for example, on a boarder of grain, where the ions experience different local electric fields. Taking into account volume to surface ratio, which is very small compared to micro-sized samples, those ions which are placed on the surface of the nanocrystallite play an important role. The broad emission lines are also observed in glasses or other amorphous compounds. In single crystals ions occupy only specific sites in the crystal structure and the amount of ions placed on the surface is negligible.

The luminescence spectrum of neodymium in our host lattice is presented in Fig. 7. This spectrum was measured on CCD camera, which gives an accurate results for visible light, but has poorer sensitivity in the IR region (1000–1100 nm). Therefore, on this picture the most intensive is the $^4F_{3/2} \rightarrow {}^4I_{9/2}$ transition. Fig. 8 presents a spectrum measured an InGaAs detector which is more appropriate for the near infrared range.

The Stark levels of neodymium in $CaTiO_3$ are presented in Table 2. At room temperature the emission from both $^4F_{3/2}$ levels to the ground state is strong. At 77 K, peaks which correspond to a transition from the higher Stark $^4F_{3/2}$ energy level are much weaker. The $(^4F_{5/2}+{}^2H_{9/2}) \rightarrow {}^4I_{9/2}$ emission at about 810 nm occurs only at room temperature, because this emitting level is thermally populated from the $^4F_{3/2}$ level.

The emission decay profile of the $^4F_{3/2}$ level is single exponential and mostly depends on the concentration of neodymium, less on the crystallite size and temperature of measurement. The increasing amount of Nd^{3+} ions causes decreasing lifetime of the $^4F_{3/2}$ level (see Fig. 9). Above 1% of Nd^{3+} decay time drops almost two times. The concentration quenching is due to almost resonant cross-relaxation (CR) process:

$$(^4F_{3/2},{}^4I_{9/2}) \rightarrow ({}^4I_{15/2},{}^4I_{15/2}),$$
$$(11512,0) \rightarrow (5773,5773) - 34\,cm^{-1}$$

A CR process is possible for two closely spaced ions. The probability of the existence of these pairs is proportional to the growing concentration of doped ions.

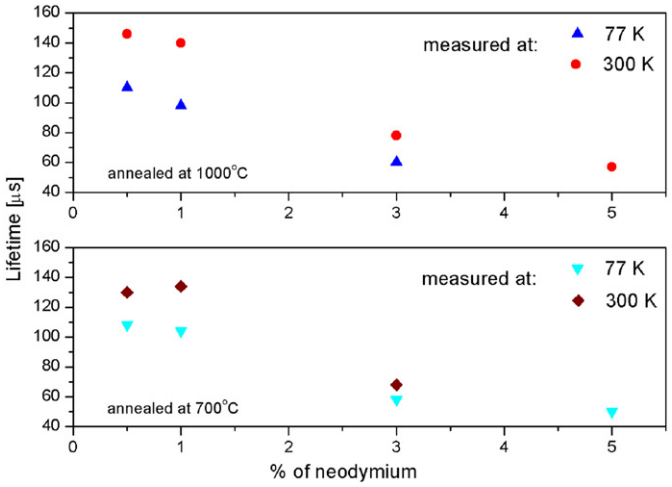

Fig. 9. Lifetime of the $^4F_{3/2}$ level as a function of Nd^{3+} concentration in $CaTiO_3$.

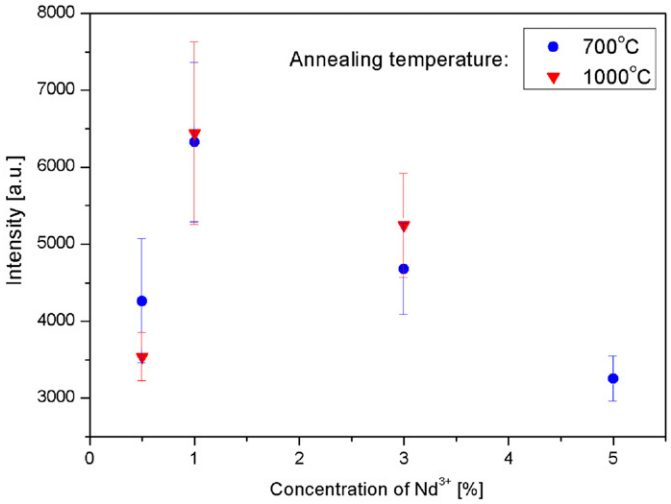

Fig. 10. Intensity of the $^4F_{3/2} \rightarrow {}^4I_{9/2}$ transition of neodymium in $CaTiO_3$ nanocrystals with the experimental errors.

The lifetime of the $^4F_{3/2}$ energy level of neodymium at room temperature is slightly longer than the lifetime measured at 77 K. This phenomenon was already observed for other crystals doped with neodymium ions [11,17].

At room temperature, both Stark components of the $^4F_{3/2}$ level emit. Lifetime of the $^4F_{3/2}$ levels is thus described by the following equation:

$$\tau_{rad} = \frac{1+e^{-\Delta E/kT}}{(1/\tau_1)+(1/\tau_2)e^{-\Delta E/kT}} \quad (1)$$

where, τ_1 is the lifetime of the lower laying Stark component and τ_2 is the lifetime of the higher component of the $^4F_{3/2}$ level. Energy separation between them is $\Delta E = 103\ cm^{-1}$ (see Table 2). For calculation we took for τ_1 the decay time measured at 77 K. The lifetime τ_2 estimated from the Equation (1) is equal to 345 μs, which is quite similar to values obtained by the other authors [11,17]. The estimation has been made for samples with the lowest concentration of neodymium to avoid the errors caused by the influence of the CR process.

The intensity of neodymium photoluminescence has been compared to the most intensive and stable peak at 876.6 nm of the $^4F_{3/2} \rightarrow {}^4I_{9/2}$ transition. The average emission intensity for the 700 °C and 1000 °C samples is strongest for the 1% concentration of doped neodymium. For higher amounts of dopant, concentration quenching occurs (see Fig. 10), due to the increased number of Nd–Nd pairs. Indeed, most of the commercially available laser crystals based on emission of neodymium ions have a concentration of about 1% of this lanthanide.

The *spectroscopic quality parameter* X_{Nd} was defined as a ratio of Judd–Ofelt intensity parameters Ω_4/Ω_6 [18]. It is possible to calculate it from the emission spectra measured at room temperature (see Fig. 8). The formula to calculate X_{Nd} from luminescence data has been described by Kaminskii [18]

$$X_{Nd}(^4F_{3/2}) = 0.765 Y_{Nd} - 2.96,$$

where $Y_{Nd} = I_{J,11/2}/I_{J,13/2}$

and I_J is the integrated luminescence intensities; J is a total angular momentum quantum number.

Depending on the sample the X_{Nd} has a different value in the range from about 0.6 to 1.8 (Fig. 11). The Judd–Ofelt parameters are host dependent but do not depend on concentration, so differences in X_{Nd} values indicate that host lattices are not identical. Hypersensitive transitions owe their name to their high

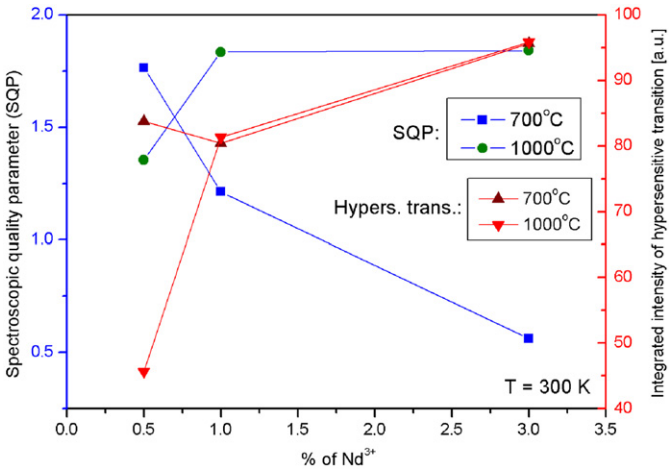

Fig. 11. The values of the spectroscopic quality parameter obtained for Nd^{3+} in $CaTiO_3$; together with integrated values of the $^4I_{9/2} \rightarrow {}^4G_{5/2}$ hypersensitive transition normalized to the $^4I_{9/2} \rightarrow {}^4F_{7/2}$ transition as a function of Nd^{3+} concentration.

sensitivity to the environment. Their intensity as a function of Nd^{3+} concentration changes in the same way as the X_{Nd} (see Fig. 11). The differences in the local structure are caused by the amount of doped Nd^{3+}, which substitute ions with different valences and sizes. The valence mismatch introduces structural defects like calcium or oxygen vacancies, reducing Ti^{4+} to Ti^{3+} and forming TiO_6 and TiO_5 clusters [12]. Hanajiri et al. [19] analyzed the influence of dopant (neodymium and cerium) on the local structure of $CaTiO_3$ powder. Using the EXAFS technique they showed that with higher Nd^{3+} content, the Ti–O distances decrease whereas the Nd–O distances increase, which changes the strengths of the local crystal field of the Nd^{3+} ions.

Using the method described by Kaminskii we obtained the branching ratio of emission from $^4F_{3/2}$ to ^4I_J levels. The contribution of the emission depending on the percentage of doped neodymium is steady for almost all nanocrystallites, only for samples with 0.5% of Nd^{3+} does it differ. For these nano-powders, slight changes are observed for the branching ratio from $^4F_{3/2}$ to the ground and first excited level (see Fig. 12).

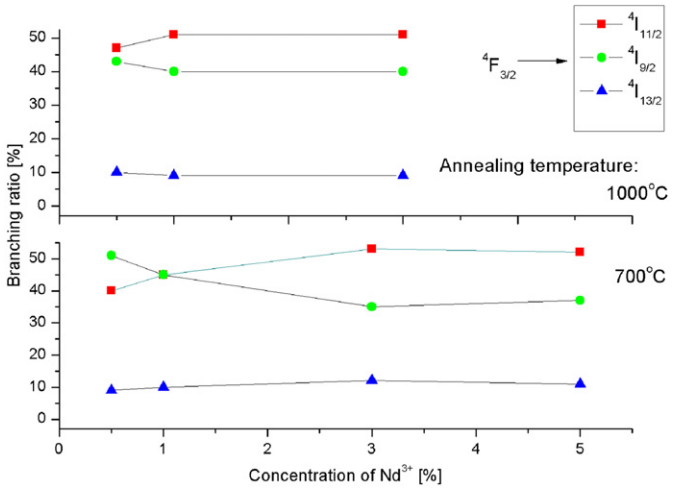

Fig. 12. Branching ratio of the emitting levels of Nd^{3+} in $CaTiO_3$ nanocrystals as a function of Nd^{3+} concentration.

4. Conclusions

We presented a new nano-sized host lattice for neodymium ions which possesses a good luminescent properties and might be used for different photonic applications. The excitation, absorption, VIS–NIR emission spectra and time decay profile of the $^4F_{3/2}$ energy level of Nd^{3+} in $CaTiO_3$ nanocrystallites have been obtained for the first time. For this nano-perovskite a strong luminescence of neodymium ions has been observed.

The emission from the $^4F_{3/2}$ to the $^4I_{9/2}$ and also the $^4I_{11/2}$ terms dominate in the spectra. The strongest luminescence occurred for a 1% concentration of Nd^{3+}. However, the 700 °C and 1000 °C samples showed almost the same emission intensity. The lifetime of $^4F_{3/2}$ significantly decreases for samples with concentrations of neodymium higher than 1% due to the concentration quenching caused by the virtually resonant cross-relaxation process.

The obtained samples are pure single phase materials. The dopant Nd^{3+} ions substitute for Ca^{2+} on the C_s symmetry site. An increased concentration of neodymium strongly influences the emission properties of the $CaTiO_3$ perovskite. Cell parameters grow with the growing dopant content. The changes in the crystal structure of $CaTiO_3$ hosts are manifested by the changes in the emission spectra.

Acknowledgments

This work was supported by the Polish Committee for Scientific Research (KBN) within Project number: N N507 372335.

Appendix A. Supporting material

Supplementary data associated with this article can be found in the online version at doi:10.1016/j.jssc.2011.08.004.

References

[1] E. Roduner, Chem. Soc. Rev. 35 (2006) 583.
[2] A. Boudali, A. Abada, M. Driss Khodja, B. Amrani, K. Amara, F. Driss Khodja, A. Elias, Physica B 405 (2010) 3879.
[3] L. Sarakh, A. Bousquet, E. Tomasella, P. Boutinaud, R. Mahiou, Mater. Sci. Eng. 12 (2010) 012008.
[4] P. Li, S. Karato, S, Z. Wang, Phys. Earth Planet. 95 (1996) 19.
[5] R.C. Kell, A.C. Greenham, G.C.E. Olds, J. Am. Ceram. Soc. 56 (1973) 352.
[6] J. Nowotny, M. Rekas, in: J. Nowotny (Ed.), El. Cer. Mat., 89, Trans Tech Publ., Zurich, 1992.
[7] Y. Arita, K. Nagarajan, T. Ohashi, T. Matsui, J. Nucl. Mater. 246 (1997) 94.
[8] M. Manso, M. Langlet, J.M. Martinez-Duart, Mater. Sci. Eng. C 23 (2003) 447.
[9] S.S. Chadha, D.W. Smith, A. Vecht, C.S. Gibbons, SID 94 Digest (1994) 51.
[10] B.J. Kenndey, C.J. Howard, B.C. Chakoumakos, J. Phys.: Condens. Matter 11 (1999) 1479.
[11] P.J. Dereń, A. Bednarkiewicz, Ph. Goldner, O. Guillot-Noel, J. Appl. Phys. 103 (2008) 043102.
[12] V.S. Marquesa, L.S. Cavalcanteb, J.C. Sczancoski, E.C. Paris, J.M.C. Teixeiraa, J.A. Varela, F.S. De Vicente, M.R. Joya, P.S. Pizani, M. Siu Li, M.R.M.C. Santos, E. Longo, Spectr. Acta Part A 74 (2009) 1050.
[13] P.J. Dereń, R. Pązik, W. Stręk, Ph. Boutinaud, R. Mahiou, J. All. Compd. 451 (2008) 595.
[14] V. Petricek, M. Dusek, L. Palatinus, Jana2000. Structure Determination Software Programs, Institute of Physics, Praha, Czech Republic, 2000.
[15] P. Scherrer, Gottinger Nachr. 2 (1918) 98.
[16] C.-M. Wang, J. Cho, H.M. Chan, M.P. Harmer, J.M. Rickman, J. Am. Ceram. Soc. 84 (2001) 1010.
[17] I. García-Rubio, J.A. Pardo, R.I. Merino, R. Cases, V.M. Orera, J. Lumin. 86 (2000) 147.
[18] A.A. Kaminskii, Crystalline lasers: Physical Processes and Operating Schemes, CRC Press, New York, 1996.
[19] Y. Hanajiria, T. Matsuia, Y. Aritaa, T. Nagasakia, H. Shigematsu, T. Harami, Solid State Ionics 108 (1998) 343.